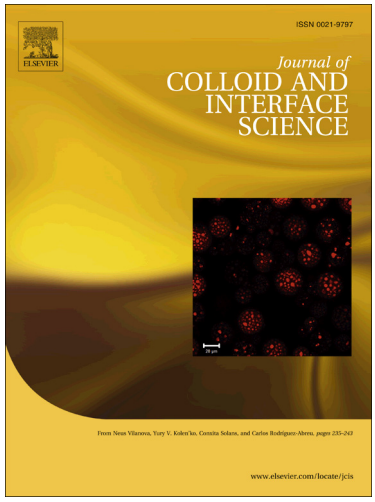

High-performance glucose biosensor based on chitosan-glucose oxidase immobilized polypyrrole/Nafion/functionalized multi-walled carbon nanotubes bio-nanohybrid film

Bishnu kumar Shrestha, Rafiq Ahmad, Hamouda M. Mousa, In-Gi Kim, Jeong In Kim, Madhav Prasad Naupane, Chan Hee Park, Cheol Sang Kim

PII: S0021-9797(16)30533-1
DOI: http://dx.doi.org/10.1016/j.jcis.2016.07.067
Reference: YJCIS 21453

To appear in: *Journal of Colloid and Interface Science*

Received Date: 4 May 2016
Revised Date: 25 July 2016
Accepted Date: 26 July 2016

Please cite this article as: B.k. Shrestha, R. Ahmad, H.M. Mousa, I-G. Kim, J.I. Kim, M.P. Naupane, C.H. Park, C.S. Kim, High-performance glucose biosensor based on chitosan-glucose oxidase immobilized polypyrrole/ Nafion/functionalized multi-walled carbon nanotubes bio-nanohybrid film, *Journal of Colloid and Interface Science* (2016), doi: http://dx.doi.org/10.1016/j.jcis.2016.07.067

High-performance glucose biosensor based on chitosan-glucose oxidase immobilized polypyrrole/Nafion/functionalized multi-walled carbon nanotubes bio-nanohybrid film

Bishnu kumar Shrestha[1,2], Rafiq Ahmad[3], Hamouda M. Mousa[1,4], In-Gi Kim[1], Jeong In Kim[1], Madhav Prasad Naupane [1], Chan Hee Park[1,2]*, Cheol Sang Kim[1,2,]*

[1] Department of Bionanosystem Engineering, Graduate School, Chonbuk National University, 567 Baekje-daero, Deokjin-gu, Jeonju-si, Jeollabuk-do 54896, Republic of Korea.

[2] Division of Mechanical Design Engineering, Chonbuk National University, 567 Baekje-daero, Deokjin-gu, Jeonju-si, Jeollabuk-do 54896, Republic of Korea.

[3] School of Semiconductor and Chemical Engineering, Nanomaterials Processing Research, Chonbuk National University, 567 Baekje-daero, Deokjin-gu, Jeonju-si, Jeollabuk-do 54896, Republic of Korea.

[4] Department of Engineering Materials and Mechanical Design, Faculty of Engineering, South Valley University, Qena 83523, Egypt.

*Authors to whom corresponding should be addressed.

E-mail: chskim@jbnu.ac.kr, biochan@jbnu.ac.kr, Tel.: +82-63-270-4284, Fax: +82-63-270-2460.

Abstract

A highly electroactive bio-nanohybrid film of polypyrrole (PPy)-Nafion (Nf)-functionalized multi-walled carbon nanotubes (fMWCNTs) nanocomposite was prepared on the glassy carbon electrode (GCE) by a facile one-step electrochemical polymerization technique followed by chitosan-glucose oxidase (CH-GOx) immobilization on its surface to achieve a high-performance glucose biosensor. The as-fabricated nanohybrid composite provides high surface area for GOx immobilization and thus enhances the enzyme-loading efficiency. The structural characterization revealed that the PPy-Nf-fMWCNTs nanocomposite films were uniformly formed on GCE and after GOx immobilization, the surface porosities of the film were decreased due to enzyme encapsulation inside the bio-nanohybrid composite materials. The electrochemical behaviour of the fabricated biosensor was investigated by cyclic voltammetry (CV), electrochemical impedance spectroscopy (EIS), and amperometry measurements. The results indicated an excellent catalytic property of bio-nanohybrid film for glucose detection with improved sensitivity of 2860.3 μAmM^{-1} cm^{-2}, the linear range up to 4.7 mM (R^2 =0.9992), and a low detection limit of 5 μM under a signal/noise (S/N) ratio of 3. Furthermore, the resulting biosensor presented reliable selectivity, better long-term stability, good repeatability, reproducibility, and acceptable measurement of glucose concentration in real serum samples. Thus, this fabricated biosensor provides an efficient and highly sensitive platform for glucose sensing and can open up new avenues for clinical applications.

Keywords: Polypyrrole; Multi-walled carbon nanotubes; Electrochemical polymerization; Bio-nanohybrid; Glucose biosensor

1. Introduction

A comprehensive approach for early detection of diabetes mellitus is urgently needed to assess the risk, diagnosis, and further management of several diseases causing adverse effect on human health. It is well known that dysfunction or diminished effectiveness of endogenous insulin secretion by the pancreatic β-cells increases the blood glucose level for prolong period, which predominantly results in heart attacks, stroke and amputations, and proteinuria contributing to higher mortality rate in recent years [1]. To overcome the increasing demands for early monitoring and detection of diabetes, numerous strategies have been studied extensively over the past several years [2-5]. Among all, glucose detection based on electrochemical technique is particularly cited as a feasible platform to achieve excellent specificity, accuracy, reliability, and interference free assays [6].

Various forms of nanomaterials have been extensively utilized for the fabrication of electrochemical based glucose biosensors [7-12]. Among them, composite materials offer several distinctive benefits over traditional materials; as they provide super electrical conductivity, biocompatibility, strong mechanical strength, thermal and chemical stability, large surface area to volume ratio and low mass density [13]. Composite materials including carbon nanotubes (CNTs) and metal/metal oxide nanostructures have received much attention over the past decade as sensing elements for nano-engineered biosensors, which enhance the electron transfer rate during electrochemical reaction due to high surface-to-volume ratio by catalyzing the biomolecules, like dopamine, protein, glucose, uric acid, and ascorbic acid [14]. On the other hand, electroactive conducting polymers (EACPs) and their derivatives have shown excellent physical, electrochemical, and biological response [15-17]. Especially, polypyrrole (PPy) as EACPs has been actively researched as a potential material for biosensor fabrication because of its easily

synthesis, rapid electron transport, chemical stability, environmental stability, good mechanical properties, low ionization potential, high electron affinity, and promising biocompatibility under physiological conditions [18]. Thus, incorporation of PPy on functionalized multi-walled carbon nanotubes (fMWCNTs) not only enhances the catalytic properties but also improves the enzyme-loading efficiency. The carboxylic groups on fMWCNTs also help to directly immobilize the GOx via covalent linkage, which further provide stability to the fabricated electrode. In addition, PPy acts as an effective redox mediator that reinforces to shuttle electrons from flavin adenine dinucleotide (FAD) centers within GOx to electrode surface that improves the biosensor performances [19].

To date, composite materials based on fMWCNTs with EACPs have been utilized for GOx immobilization through physical adsorption and entrapment methods [20,21]. However, such non-covalent methods results in decreased enzyme activity and poor stability of electrodes. Thus, a biosensor with significant architecture is needed with comprehensive improved sensing properties i.e. high sensitivity, fast response, high stability and lower potential of redox reaction. Herein, we fabricated a highly electroactive bio-nanohybrid film of PPy-Nf-fMWCNTs on GCE surface by a facile one-step in situ electrochemical polymerization technique and sequentially used for the CS-GOx immobilization to design high performance glucose biosensor. The Nf used during sensor fabrication reduces the aggregation of fMWCNTs in electrolytic solution during electro-polymerization. The nanohybrid film provided high surface area for GOx immobilization and good electron transport path, which further led to an outstanding catalytic property for glucose detection. Importantly, the fabricated biosensor showed high sensitivity for glucose detection. Thus, using this biosensor would avert the requirement of drawing a lot of blood for analysis. A small amount of diabetic patients blood/serum can be diluted and used for the glucose

concentration measurement. In addition, the fabricated sensors were utilized to detect glucose in real serum samples.

2. Experimental details

2.1. Reagents

The heterocyclic organic compound pyrrole (C_4H_5N, 99% purity) was purchased from Daejung-Korea. The MWCNTs (95% purity Ca.10 nm in external diameter) prepared by chemical vapor deposition (CVD) were obtained from Nanosolution Co. Ltd. Korea. Glucose oxidase (GOx, EC 1.1.3.4, Type X-S 127 unit/mg, *Aspergillus niger*), Nafion (Nf, 5 wt. % in the mixture of lower aliphatic alcohol with water), dopamine (DA), uric acid (UA), acetic acid (CH_3COOH), sulfuric acid (H_2SO_4), nitric acid (HNO_3), acetonitrile (CH_3CN), and chitosan (CH) a linear polysaccharide with 75%-85% deacetylation, viscosity of 1% solution in 1% acetic acid = 200-800 cps in medium molecular weight, and potassium ferricyanide ($K_3[Fe(CN)_6]$ were obtained from Sigma-Aldrich (Korea). Glucose and ascorbic acid (AA) were purchased from Tokyo chemical industry Co. Ltd from Bioshop Canada Inc. Na_2HPO_4, KH_2PO_4 and KCl were purchased from Samchun Pure Co. Ltd (Korea). All chemicals used were of analytical grade and used as received without any further purification. Phosphate buffer solution (PBS, 0.1 M, pH 7.4) was freshly prepared in ultrapure water purified using a Millipore-Q system.

2.2. Synthesis of bio-nanohybrid film and characterization

For the preparation of bio-nanohybrid film, first, 0.5 gm of as-obtained pristine multi-walled carbon nanotubes (MWCNTs) were added in a round bottom flask containing the mixture of concentrated sulfuric acid (120 mL) and nitric acid (40 mL). The obtained mixture was sonicated for 30 min before refluxing at 90 °C for 24 h with continuous magnetic stirring [22]. The resulting

mixture was washed with deionized (DI) water with sufficient dilution after 72 h for complete generation of carboxylic acid group having pH equivalent DI water. The formation of carboxylic groups on sidewalls have tendency to form hydrogen bonds and covalent bonds with other chemical moieties. Then, a homogenous distribution of fMWCNTs was achieved by dissolving 1 mg/mL fMWCNTs in 10 mL aqueous acetonitrile solution (1 M) containing 200 µL of 0.05 % Nf. The resultant solution was ultra-sonicated for 30 min at room temperature followed by addition of 0.1 M pyrrole and again sonication for 30 min at normal temperature and pressure. In the next step, glassy carbon electrode (GCE) was taken and polished with 0.3 and 0.05 µm alumina slurries followed by 0.25 µm diamond suspensions on rayon polishing pads prior to the modification with bio-nanohybrid materials. All polishing steps required extensive rinsing before treating ultra-sonication into ethanol for 15 min. The electrodes were cleaned with DI water and dried under nitrogen atmosphere. Finally, in situ electrochemical polymerization was carried out to deposit the nanohybrid film of PPy-Nf-fMWCNTs on GCE using three electrodes electrochemical cell in the potential range from -0.4 to +0.8V (*vs.* standard calomel electrode (SCE)) at the scan rate of 50 mV/sec for 25 cycles. The anodic polymerization of pyrrole produces PPy that could form hydrogen bonds with carbonyl groups of fMWCNTs, which contributes mechanical stability and proper conjugation to the nanohybrid composites [23]. The modified electrodes were washed sequentially with DI water to remove loosely attached PPy and fMWCNTs and dried at room temperature for 4 h before glucose oxidase immobilization.

The general morphologies of as-obtained fMWCNTs and synthesized bio-nanohybrid films were characterized by field emission scanning electron microscopy (FESEM; Carl Zeiss SUPRA 40VP, Germany) equipped with an energy dispersive spectroscopy (EDS) and Cs-corrected scanning transmission electron microscope (Cs-STEM; JEOL/JEM-ARM200F). Furthermore, the

absorption of infrared radiation by the composite material was analyzed by Fourier transmission infrared spectrometer (FTIR, Perkin Elmer, Spectrum GX, USA) and Raman spectroscopy (Nanofinder 30,Tpkyo Instrument Inc.). The UV-visible spectra were recorded using spectrophotometer (UV-2450, SHIMADZU CORP.)

2.3. Fabrication of glucose biosensor and measurements

Fig. 1 shows the schematic of glucose biosensor fabrication strategy. First, 1 mg/mL of GOx prepared in 0.1 M PBS (pH 7.4) solution was mixed with 0.5 wt % CH prepared in 1 % aqueous acetic acid in the ratio of 2:1 v/v and kept for 12 h at 4 °C. Then, 5 µL of CH-GOx suspension was casted onto the surface of modified GCE electrode and kept at 4 °C for overnight. Finally, as prepared electrodes (CH-GOx/PPy-Nf-fMWCNTs/GCE) were washed with PBS to remove loosely attached enzymes and stored in 0.1 M PBS (pH 7.4) at 4 °C when not in use.

All electrochemical measurements were performed on a ZIVE SP1 potentiostat/galvanostat/EIS electrochemical workstation (WonATech Co. Ltd. Seoul, Korea) at normal temperature and pressure. A conventional three-electrode electrochemical system was utilized, which includes a modified GCE (0.071 cm^2) as the working electrode, a platinum wire as the counter electrode, and a standard calomel electrode (SCE) as reference electrode. The cyclic voltammetry (CV) and amperometry measurements were performed in 10 mL of 0.1 M PBS (pH 7.4) solution. All experimental solutions were purged with high purity nitrogen for 15 min prior to each measurement. The Galvanostatic electrochemical impedance spectroscopy (EIS) of bio-nanohybrid biosensors were measured in 0.1 M PBS at an amplitude of 1 mV and the frequency from 0.1 Hz to 1 MHz.

3. Results and discussion

3.1. Structural characterizations

Fig. 2(a-f) presented the FESEM images of GCE modified with different nanohybrid composite films deposited by electrochemical polymerization technique. As seen in Fig. 2(a), the anodic oxidation of pyrrole produced PPy that was uniformly covered on GCE surface and has tubular array with nanopore structure in vertical orientation. Fig. 2(b & c) show the fMWCNTs decorated with PPy in the absence and presence of Nf, respectively. Fig. 2 (d-f) shows the FESEM images after CH-GOx immobilization on PPy (d), PPy-fMWCNTs (e) and PPy-Nf-fMWCNTs (f) along with their EDS data in respective insets. The porosity of film was decreased after CH-GOx immobilization due to enzyme encapsulation inside the nanohybrid composite film; as a result smooth surface of modified electrodes were obtained. The EDS data confirms the formation of nanohybrid composite and showed that the electrochemical polymerization of pyrrole in the presence of Nf enhances the enzyme immobilization capacity with cationic redox polymer like chitosan, which further improves the chemical and physical stability of the biosensor [24]. As well, the homogenous integration of PPy on fMWCNTs along with Nf exhibits synergetic effects on the electron transfer rate, which increases the diffusion-controlled reduction currents of fabricated biosensor electrode [25]. Moreover, the hydrophilicity of sulfonic groups in polymer chain of Nf also provides high surface area to volume ratio for enzyme loading during sensor fabrication. The Nf not only played an important role for well dispersion of fMWCNTs but also helped to form strong supramolecular composite between PPy and fMWCNTs through hydrogen bonds that enables the homogeneity of PPy-Nf-fMWCNTs films.

Furthermore, fMWCNTs and PPy decorated fMWCNTs were examined by CS-Corrected-FETEM/STEM as shown in Fig. 3. The low (Fig. 3a) and high (Fig. 3b and c) magnification images obtained from CS-Corrected-FETEM/STEM showed smooth surface morphology with

reduced diameter (~8.54 nm) of fMWCNTs from 10 nm pristine MWCNTs during acid functionalization (Fig. 3b). The integration of PPy on fMWCNTs was observed by mapping of PPy decorated fMWCNTs (Fig. 3c), which showed that the surfaces of fMWCNTs were decorated with PPy (circled in yellow colour).

The FTIR spectra were recorded to verify the PPy grafting on the surface of fMWCNTs through weak hydrogen bonds. Fig. 4 shows the FTIR spectra of fMWCNTs (a), PPy (b), and PPy-Nf-fMWCNTs nano-hybrid composites (c). The characteristic peaks centered at 3423 and 2398 cm^{-1} depicts the presence of O-H stretching and strong hydrogen bonds of -COOH groups on the sidewall of fMWCNTs as shown in Fig. 4a [26]. More significant peaks were appeared at 1704 cm^{-1} and 1214 cm^{-1} are assigned to C=O and C-O stretching, respectively. In addition, the evidence of symmetric and asymmetric vibration of -COO group was supported by the presence of two peaks at 1384 cm^{-1} and at 1620 cm^{-1} [27]. The FTIR spectra of PPy (Fig. 4b) shows a strong peak at 3180 cm^{-1}, which is assigned to the N-H stretching. Two peaks at around 787 to 932 cm^{-1} are assigned to =C-H out-of-plane deformation and at 1040 cm^{-1} with respect to C-H in-plane deformation. Furthermore, the intense bands at 1569 cm^{-1} and 1183 cm^{-1} correspond to C=C ring stretching and C-N symmetric stretching vibrational mode, respectively [28]. The spectra of PPy-Nf-fMWCNTs nano-hybrid composites (Fig. 4c) shows a broad peak at 3430 cm^{-1} that may be associated with the formation of hydrogen bonds between C=O groups on fMWCNTs with N-H position of PPy [29]. Moreover, two peaks at 1156 cm^{-1} and 961cm^{-1} are due to the presence of Nf in the composite, which correspond to the C-F and C-O-C symmetric stretching, respectively [30].

The electronic state and vibrational spectra of fMWCNTs, PPy, and PPy-Nf-fMWCNTs nano-hybrid composites were characterized by Raman spectroscopy (Fig. 5). The typical bands at 1356

cm^{-1} and 1586 cm^{-1} indicate the D-band in hexagonal framework and G-band along with graphite nano-sheet in tangential mode of fMWCNTs, respectively (Fig. 5a) [31]. The characteristic peak of D-band intended to the defect or disorders induced due to the presence of oxygen groups as well as diamond like carbon in SP^3 hybridization with A_{1g} of breathing mode in C-C bonds. Moreover, the G-band is assigned from in-plane E_{2g} stretching vibration mode with graphite carbon in SP^2 configuration [32]. The higher value of peaks intensity ratio of D-band (I_D) to G-band (I_G) correspond to the presence of more defects on side walls of oxidized MWCNTs [33]. The most oxidized state of PPy which could examine the charge distribution, redox properties, and state of conjugation was confirmed by the presence of Raman peaks at 935 cm^{-1} (C-H, symmetrical out-of-plane), 1054 cm^{-1} (in-plane bending), and at 1087 cm^{-1} (Fig. 5b) [34]. Furthermore, the broad band at ~1330 cm^{-1} (C-C stretching), ~1416 cm^{-1} (C-N stretching mode) and at 1587 cm^{-1} (C=C backbone stretching) explain the superior electrical conductivity of PPy [35]. Furthermore, Raman spectra of PPy-Nf-fMWCNTs nano-hybrid composite (Fig. 5c) showed a low intensity peak at 786 cm^{-1}, which suggests formation of the hydrogen bonds between fMWCNTs with PPy [36]. Noteworthy, all bands at 741 cm^{-1} and 783 cm^{-1} assigned to CF_2 symmetric stretching and C-C-C linear chains, respectively [37]. In addition the symmetric stretching modes of SO_3^{-1} groups and C-O-C side chain skeleton are located at 1048 cm^{-1} and 971 cm^{-1}, respectively, that confirms the presence of Nf in composite material [38]. The slight shift of G-band (1572 cm^{-1}) indicates electrical conductivity enhancement of composite film associated with the charge transfer from fMWCNTs in π state to dopant species of PPy (Fig. 5c) [39].

Fig. 6 shows the UV-Visible spectra of fMWCNTs (a), PPy (b), and PPy-Nf-fMWCNTs nano-hybrid composites (c). A small peak appeared at ~312 nm corresponds to the n-π^* transition of unshared paired of electrons in -COOH groups of fMWCNTs (Fig. 6a). The characteristic peaks

appeared at ~240 nm and ~488 nm of PPy (Fig. 6b) are assigned to π conjugation in Py ring within C=C stretching and the transition between valance bond and the anti-banding polaron or bipolaron transition state, respectively [40]. Furthermore, two absorption peaks at ~286 nm and ~508 nm are observed in the spectra of nano-hybrid composite material (Fig. 6c), which showed a red shift compared to oxidized PPy (Fig. 6b). The displacement of peaks position towards the direction of higher wavelength confirm the fMWCNTs doping with polymer, as a result the active surface area and conductivity of nano-hybrid composite was enhanced [41].

3.2. Electrochemical characterizations

3.2.1 Electrochemical characterization of the different modified electrodes

In order to verify the electrochemical activity of surface modified electrodes, the EIS of (a) CH-GOx/PPy/GCE, (b) PPy/GCE, (c) CH-GOx/PPy-fMWCNTs/GCE, (d) PPy-fMWCNTs/GCE, (e) CH-GOx/PPy-Nf-fMWCNTs/GCE and (f) PPy-Nf-fMWCNTs/GCE electrodes were measured in 0.1 M PBS (pH 7.4). Fig. 7 shows the typical Nyquist plots acquired from the modified electrodes. A Randles circuit was used to fit the EIS data (see upper inset of Fig. 7), indicating the solution resistance (R_{sol}), double layer capacitance (C_{dl}), charge transfer resistance (R_{ct}) and diffusion element known as Warburg impedance (Z_w). A small semicircular domain at high frequencies and a straight line at low frequencies correspond to the electron transfer limited process and diffusion process, respectively. Next, the R_{ct} values of different modified electrodes were compared with or without CH-GOx immobilization. The significant decrease in R_{ct} value of PPy-Nf-fMWCNTs/GCE (121.69 Ω, curve f) with respect to PPy-fMWCNTs/GCE (214.35 Ω, curve d) and PPy/GCE (779.10 Ω, curve b) was attributed to the microstructures, increase in specific surface area and influence of the electroconductivity of both Nf and fMWCNTs [42]. A

considerable increase in R_{ct} values of CH-GOx/PPy-Nf-fMWCNTs/GCE (151.71 Ω, curve e), CH-GOx/PPy-fMWCNTs/GCE (277.13 Ω, curve c) and CH-GOx/PPy/GCE (1133.74 Ω, curve a) and decrease in slop of straight lines confirm the successful immobilization of CH-GOx on bio-nanohybrid composite which slightly decreases the electron transfer and diffusion process of the matrix.

3.2.2. Electrochemical behavior of CH-GOx/PPy-Nf-fMWCNTs/GCE biosensor electrode

The electrochemical characteristics of the GOx-CH/PPy-Nf-fMWCNTs/GCE biosensor electrodes were studied by CV using $[Fe(CN)_6]^{3-/4-}$ solution as the redox mediator. Fig. 8(a) depicts typical CVs of GOx-CH/PPy-Nf-fMWCNTs/GCE at different scan rates in 5 mM $[Fe(CN)_6]^{3-/4-}$ with 0.1 M KCl prepared in 0.1 M PBS (pH 7.4). The obtained average anodic peak-to-cathodic peak separation (ΔE_p = ~136 mV) indicates that the modified electrode exhibits quasi-reversible electron transfer process. The larger value of peaks separation indicates presence of more active sites on the surface of composite film with higher electrocatalytic activities. Furthermore, the peaks width increases due to the strong immobilization of CH-GOx, which assists the small hindrance for the transfer of charges/electrons. The presence of thin film of Nf resists the interference of anionic biomolecules creating high partition coefficient of redox compound having synergetic effect on higher peak current along with fMWCNTs. With increasing CVs scan rate (25-250 mV/s), the anodic and cathodic peak currents are linearly proportional to the square root of the scan rates with high regression coefficient values (Fig. 8(b)). Moreover, the increase in peak-to-peak separation indicates the limitation arising from charge transfer kinetics rather than diffusion process [43].

3.2.3. Electrocatalytic activities of fabricated biosensor electrodes

The electrocatalytic activities of CH-GOx/PPy/GCE, CH-GOx/PPy-fMWCNTs, and CH-

GOx/PPy-Nf-fMWCNTs/GCE biosensor electrodes were examined through CV in the potential range of -0.2 to +0.8 V in 0.1M PBS (pH 7.4). In Fig. 9, the CV response showed an increased current in the presence of 2.0 mM glucose (solid lines), while no peaks were observed in the absence of glucose (dash lines) in PBS solution. A remarkable increase in oxidation peak current (496 µA) at +0.25 V was observed for CH-GOx/PPy-Nf-fMWCNTs (curve f) modified GCE electrode, which was ~1.8 times higher than the oxidation peak current (281 µA) obtained form CH-GOx/PPy-fMWCNTs (curve d) modified GCE electrode. Noteworthy, the presence of Nf provides effective and chemically stable high surface area by homogenously distributing the fMWCNTs that may combine with biopolymer containing covalently immobilized GOx. The possible mechanism of electrocatalytic oxidation of glucose could be expressed as following [5].

β-D-Glucose + GOx(-FAD) → D-Glucono-1-5-lactone + GOx-$FADH_2$ (1)

GOx-$FADH_2$ + O_2→ GOx-FAD + H_2O_2 (2)

$H_2O_2 \rightarrow 2H + O_2 + 2e^-$ (3)

3.3. Amperometric detection of glucose

We further used fabricated biosensor electrodes (CH-GOx/PPy-Nf-fMWCNTs/GCE) to evaluate the analytical performance by amperometric measurements at the applied potential of +0.25 V (*vs.* SCE) in 0.1 M PBS (Fig. 10). With successive addition of different concentrations of glucose (0.005-5.7 mM), a fast and well-defined amperometric response with an average time (~3 s) required to reach the steady-state current was observed (Fig. 10a). This shows a fast electrocatalytic process on as-fabricated electrode surface. The corresponding calibration curve of biosensor response is shown in Fig. 10b. With increased glucose concentration, the current response of the biosensor was increased and reaches a saturation state at high glucose concentration, further suggesting the saturation of enzymes active sites at those glucose levels.

The sensing performances i.e. sensitivity, correlation coefficient, linear range, and detection limit under S/N ratio of 3 were calculated. The biosensor showed large linear range from 0.01 mM to 4.7 mM with high correlation coefficient (R^2 =0.9992), highest sensitivity of 2860.3 $\mu AmM^{-1}cm^{-2}$, and low detection limit of 5 μM (inset of Fig. 10a). As compared to previously reported PPy modified GCE-based glucose biosensors (Table 1), the present biosensor holds remarkably high sensitivity and wide linear range [44-48]. This indicates the excellent affinity of PPy decorated fMWCNTs in Nf for GOx immobilization, high electrocatalytic activity and conductivity, and good biocompatibility of prepared bio-nanohybrid composite film. The apparent Michaelis-Menten constant (K_M^{app}) was evaluated from the Lineweaver-Burk equation [49]: $1/i = (K_M^{app}/i_{max})(1/C) + 1/i_{max}$), where i is the steady-state catalytic current after adding substrate, i_{max} is the maximum current measured under saturation of substrate and C refer to the glucose concentration. The low (0.34 mM) K_M^{app} value assures the enzyme-substrate kinetics and also confirms the homogenous distribution of enzyme on the electrode surface for oxidizing the glucose (Fig. 10b, inset). This value is lower than the previously reported values for GOx encapsulation in polyaniline and PPy based biosensors [50,51]. This is likely due to high surface area to volume ratio of fMWCNTs and bio-friendly microenvironment of the prepared nano-hybrid composite film.

3.4. Anti-interference, reproducibility, long-term stability, and repeatability test

The anti-interference property of the CH-GOx/PPy-Nf-fMWCNTs/GCE biosensor electrodes were evaluated by measuring amperometric response with initial addition of 1.0 mM glucose and then 0.5 mM of each interfering species i.e. AA, DA, UA and again 1.0 mM glucose (Fig. 11a). A rapid response was observed upon addition of 1.0 mM glucose, whereas negligible responses were noticed after addition of interfering species (each 0.5

mM). Considering that the concentration of these interfering species in real samples are much lower than the tested concentrations, which showed that anti-interference property of our fabricated biosensor would be suitable for selective glucose detection in real human serum samples.

In addition, reproducibility of CH-GOx/PPy-Nf-fMWCNTs/GCE biosensor electrodes were examined by measuring the response current of five similar independently fabricated electrodes. The current response of each electrode was measured in a fixed concentration of glucose (1.0 mM), which showed almost similar response for all sensing devices. A low relative standard deviation (RSD=3.2%) of biosensors current response confirms excellent reproducibility of the electrode. In order to demonstrate long-term stability and repeatability of the biosensor electrode, the response to glucose were evaluated by measuring its performance after every 3 days interval as shown in Fig. 11b. The sensor was stored at 4 °C in 0.1 M PBS (pH 7.4) when not in use. The efficacy of CH-GOx/PPy-Nf-fMWCNTs/GCE electrode nearly had no change within first 21 days and after 45 days the electrodes retains about 93% of its original response to glucose. The excellent reproducibility, long-term stability, and repeatability confirm that the CH-GOx/PPy-Nf-fMWCNTs/GCE electrodes are reliable to accurately and precisely determine glucose concentrations.

3.5. Real sample detection

To explore the realistic application of the fabricated CH-GOx/PPy-Nf-fMWCNTs/GCE biosensor in practical applications, it was applied to detect the amount of glucose in human serum samples at 37 °C. As prepared biosensor was examined in 0.1 M PBS (pH 7.4, at +0.25 V) containing different concentrations of human serum samples

diluted from known glucose concentration in serum sample. Then, the recovery of glucose was determined by standard addition of pure glucose to the solutions containing the serum samples. As shown in Table 2, the measurement of glucose recovery percentage was found to be >96 % with RSD of <3.2%, indicating that the potential interfering species in serum do not affect glucose detection. The results presented from the proposed glucose biosensor were consistent with the known concentration of glucose (4.89 mM) in the human serum (Sigma-Aldrich, H4522) [52].

4. Conclusion

In conclusion, a high-performance glucose biosensor was successfully developed via one-step in situ electro-polymerization of PPy-Nf-fMWCNTs nanocomposite on GCE surface followed by CH-GOx immobilization. The as-fabricated biosensor exhibited a very high sensitivity of 2860.3 $\mu AmM^{-1}cm^{-2}$, wide-linear range up to 4.7 mM, and low detection limit of 5 µM. We found that Nf presence in the composite facilitated uniform dispersion of fMWCNTs, improved physicochemical stability, and adsorption capacity of biopolymer during enzyme immobilization. Further, the bio-nanohybrid composite (CH-GOx/PPy-Nf-fMWCNTs) provides a biocompatible environment, which increases the electrocatalytic activity of immobilized enzyme and facilitates the electron transfer rate. The cross-linking of CH with GOx prevents GOx leaching and maintains the bioactivity during operation and under storage. Additionally, the resulting biosensor exhibited excellent anti-interference ability, reproducibility, long-term storage stability, repeatability, and acceptable glucose detection in real serum samples. To sum up, these results can be envisioned to open new horizons for the fabrication of high-performance sensing devices.

Acknowledgements

This work was supported by grant from the Basic Science Research Program through National Research Foundation of Korea (NRF) by Ministry of Education Science and Technology (Project no, NRF-2013R1A2A2A04015484) and (Project No. NRF-2015R1C1A1A02036404).

References

[1] L. Melgaard, A. Gorst-Rasmussen, P. Sogaard, L.H. Rasmussen, G.Y. Lip, T.B. Larsen, Diabetes mellitus and risk of ischemic stroke in patients with heart failure and no atrial fibrillation, Int. J. Cardiac. 209 (2016) 1-6.

[2] Y.B. Hahn, R. Ahmad, N. Tripathy, Chemical and biological sensors based on metal oxide nanostructures, Chem. Commun. 48 (2012) 10369-10385.

[3] D. Zhao, C. Xu, A nanoporous palladium-nickel alloy with high sensing performance towards hydrogen peroxide and glucose, J. Colloid Interf. Sci. 447 (2015) 50-57.

[4] R. Ahmad, N. Tripathy, J.H. Park, Y.B. Hahn, A comprehensive biosensor integrated with a ZnO nanorod FET array for selective detection of glucose, cholesterol and urea, Chem. Commun. 51 (2015) 11968-11971.

[5] M.V. Jose, S. Marx, H. Murata, R.R. Koepsel, A.J. Russell, Direct electron transfer in a mediator-free glucose oxidase-based carbon nanotube-coated biosensor, Carbon 50 (2012) 4010-4020.

[6] S. Cosnier, Biomolecule immobilization on electrode surfaces by entrapment or attachment to electrochemically polymerized films, Biosens. Bioelectron. 14 (1999) 443-456.

[7] Y. Yao, H. Shen, G. Zhang, J. Yang, X. Jin, Synthesis of poly(N-isopropylacrylamide)-co-poly(phenylboronate ester) acrylate and study on their glucose-responsive behavior, J. Colloid Interf. Sci. 431 (2014) 216-222.

[8] R. Ahmad, N. Tripathy, J.H. Kim, Y.-B. Hahn, Highly selective wide linear-range detecting glucose biosensors based on aspect-ratio controlled ZnO nanorods directly grown on electrodes Sens. Actuat. B. 174 (2012) 195-201.

[9] L.T. Dipasquale, N.G. Poulos, J.R. Hall, A. Minocha, T.A. Bui, M.C. Leopold, Structure-function relationships affecting the sensing mechanism of monolayer-protected cluster doped xerogel amperometric glucose biosensors, J. Colloid Interf. Sci. 450 (2015) 202-212.

[10] R. Khan, R. Ahmad, P. Rai, L.W. Jang, J.H. Yun, Y.T. Yu, Y.B. Hahn, I.H. Lee, Glucose-assisted synthesis of Cu_2O shuriken-like nanostructures and their application as nonenzymatic glucose biosensors sensor, Sens. Actuat. B. 203 (2014) 471-476.

[11] X. Ren, D. Chen, X. Meng, F. Tang, X. Hou, D. Han, L. Zhang, Zinc oxide nanoparticles/glucose oxidase photoelectrochemical system for the fabrication of biosensor, J. Colloid Interf. Sci. 334 (2009) 183-187.

[12] K. Gong,mVertically-aligned Prussian blue/carbon nanotube nanocomposites on a carbon microfiber as a biosensing scaffold for ultrasensitively detecting glucose, J. Colloid Interf. Sci. 410 (2013) 152-157.

[13] B.H. Meshram, R.P. Mahore, P.D. Virutkar, S.B. Kondawar, Polypyrrole/carbon nanotubes/lactate Oxidase nanobiocomposite film based modified stainless steel electrode lactate biosensor, Procedia Mater. Sci. 10 (2015) 176-185.

[14] Z. Lin, J. Chen, G. Chen, An ECL biosensor for glucose based on carbon-nanotube/Nafion film modified glass carbon electrode, Electrochim. Acta 53 (2008) 2396-2401.

[15] I. Das, N. Goel, N.R. Agrawal, S.K. Gupta, Growth patterns of dendrimers and electric potential oscillations during electropolymerization of pyrrole using mono- and mixed surfactants, J. Phys. Chem. B. 114 (2010) 12888-12896.

[16] M. Gerard, A. Chaubey, B.D. Malhotra, Application of conducting polymers to biosensors, Biosens. Bioelectron. 17 (2002) 345-359.

[17] T. Ahuja, I. A. Mir, D. Kumar, Rajesh, Biomolecular immobilization on conducting polymers for biosensing applications, Biomaterials. 28 (2007) 791-805.

[18] A. Ramanavičius, A. Ramanavičienė, A. Malinauskas, Electrochemical sensors based on conducting polymer-polypyrrole, Electrochim. Acta . 51 (2006) 6025-6037.

[19] K.J. Ahn, Y. Lee, H. Choi, M.S. Kim, K. Im, S. Noh, H. Yoon, Surfactant-templated synthesis of polypyrrole nanocages as redox mediators for efficient energy storage, Sci. Rep. 5 (2015) 14097-14106.

[20] Q. Gao, Y. Guo, J. Liu, X. Yuan, H. Qi, C. Zhang, A biosensor prepared by co-entrapment of a glucose oxidase and a carbon nanotube within an electrochemically deposited redox polymer multilayer, Bioelectrochem. 81 (2011) 109-113.

[21] Y.M. Yan, I. Baravik, O. Yehezkeli, I. Willner, Integrated electrically contacted glucose oxidase/carbon nanotube electrodes for the bioelectrocatalyzed detection of glucose, J. Phys. Chem. C. 112 (2008) 17883-17888.

[22] S.D. Uzun, F. Kayaci, T. Uyar, S. Timur, L. Toppare, Bioactive surface design based on functional composite electrospun nanofibers for biomolecule immobilization and biosensor applications, ACS Appl. Mater. Interfaces. 6 (2014) 5235-5243.

[23] S. Sadki, P. Schottland, N. Brodie, G. Sabourauda, The mechanisms of pyrrole electropolymerization, Chem. Soc. Rev. 29 (2000) 283-293.

[24] G. Fortier, M. Vaillancourt, D. Bélanger, Evaluation of nafion as media for glucose oxidase immobilization for the development of an amperometric glucose biosensor, Electroanalysis 4 (1992) 275-283.

[25] D.A. Buttry, J.M. Saveant, F.C. Anson, Enhancement of charge-transport rates by redox cross-reactions between reactants incorporated in Nafion coatings, The J. Phys. Chem. 88 (1984) 3086-3091.

[26] A.S.K. Kumar, S.J. Jiang, W.L. Tseng, Effective adsorption of chromium (vi)/Cr (iii) from aqueous solution using ionic liquid functionalized multiwalled carbon nanotubes as a super sorbent, J. Mater. Chem. A. 3 (2015) 7044-7057.

[27] Z. Liu, T. Tabakman, K. Welsher, H. Dai, Carbon nanotubes in biology and medicine: In vitro and in vivo detection, imaging and drug delivery, Nano Res. 2 (2009) 85-120.

[28] L. Yuan, C. Wan, X. Ye, F. Wu, Synthesis of silver-incorporated conductive polypyrrole submicron spheres for supercapacitors, Electrochim. Acta. (2016) doi:10.1016/j.electacta.2016.06.165.

[29] H. Asadollahzadeh, E. Noroozian, S. Maghsoudi, Solid-phase microextraction of phthalate esters from aqueous media by electrochemically deposited carbon nanotube/polypyrrole composite on a stainless steel fiber, Anal. Chim. Acta. 669 (2010) 32-38.

[30] Z. Liang, W. Chen, J. Liu, S. Wang, Z. Zhou, W. Li, G. Sun, Q. Xin, FT-IR study of the microstructure of Nafion® membrane, J. Membr. Sci. 233 (2004) 39-44.

[31] V. Datsyuk, M. Kalyva, K. Papagelis, J. Parthenios, D. Tasis, A. Siokou, I. Kallitsis, C. Galiotis, Chemical oxidation of multiwalled carbon nanotubes, Carbon. 46 (2008) 833-840.

[32] C. Gao, Y.Z. Jin, H. Kong, R.L.D. Whitby, S.F.A. Acquah, G.Y. Chen, H. Qian, A. Hartschuh, S.R.P. Silva, S. Henley, P. Fearon, H.W. Kroto, D.R.M. Walton, Polyurea-

functionalized multiwalled carbon nanotubes: Synthesis, morphology, and Raman spectroscopy, J. Phys. Chem. B. 109 (2005) 11925-11932.

[33] S. Roy, T. Das, Y. Ming, X. Chen, C.Y. Yue, X. Hu, Specific functionalization and polymer grafting on multiwalled carbon nanotubes to fabricate advanced nylon 12 composites, J. Mater. Chem. A. 2 (2014) 3961-3970.

[34] C. Wang, Y. Ding, Y. Yuan, A. Cao, X. He, Q. Peng, Y. Li, Multifunctional, Highly flexible, free-standing 3D polypyrrole foam, Small, 2016. DOI: 10.1002/smll.201601905

[35] B. Zhang, Y. Xu, Y. Zheng, L. Dai, M. Zhang, J. Yang, Y. Chen, X. Chen, J. Zhou, A facile synthesis of polypyrrole/carbon nanotube composites with ultrathin, uniform and thickness-tunable polypyrrole shells, Nanoscale Res. Lett. 6 (2011) 1-9.

[36] Z. Men, W. Fang, D. Li, Z. Li, C. Sun, Raman spectra from symmetric hydrogen bonds in water by high-intensity laser-induced breakdown, Sci. Rep. 4 (2014) 4606.

[37] E.L. Pace, A.C. Plaush, H.V. Samuelson, Vibrational spectra and frequency assignments for octafluoropropane (C_3F_8) and hexafluoroacetone (C_3F_6O), Spectrochimica Acta. 22 (1966) 993-1006.

[38] J. Zeng, D. Jean, C. Ji, S. Zou, In situ surface-enhanced Raman spectroscopic studies of Nafion adsorption on Au and Pt electrodes, Langmuir 28 (2012) 957-964.

[39] F. Inoue, R.A. Ando, C.M.S. Izumi, P. Corio, Spectroscopic characterization of carbon nanotube-polypyrrole composites, J. Phys. Chem. C. 118 (2014) 18240-18248.

[40] X.H. Pham, M.P. N. Bui, C.A. Li, K.N. Han, J.H. Kim, H. Won, G.H. Seong, Electrochemical characterization of a single-walled carbon nanotube electrode for detection of glucose, Anal. Chim. Acta. 671 (2010) 36-40.

[41] T. Qian, X. Zhou, C. Yu, S. Wu, J. Shen, Highly dispersed carbon nanotube/polypyrrole core/shell composites with improved electrochemical capacitive performance, J. matter. Chem. A 1 (2013) 15230-15234.

[42] J. Hong, H. Ghourchian, A.A. Moosavi-Movahedi, Direct electron transfer of redox proteins on a Nafion-cysteine modified gold electrode, Electrochem. Commun. 8 (2006) 1572-1576.

[43] Q. Liu, X. Lu, J. Li, X. Yao, J. Li, Direct electrochemistry of glucose oxidase and electrochemical biosensing of glucose on quantum dots/carbon nanotubes electrodes, Biosens. Bioelectron. 22 (2007) 3203-3209.

[44] B. Jugović, B. Grgur, M. Antov, Z. Knežević-Jugović, J. Stevanović, M. Gvozdenović, Polypyrrole-based enzyme electrode with immobilized glucose oxidase for electrochemical determination of glucose, Int. J. Electrochem. Sci. 11 (2016) 1152-1161.

[45] M. Şenel, Simple method for preparing glucose biosensor based on in-situ polypyrrole cross-linked chitosan/glucose oxidase/gold bionanocomposite film, Mater. Sci. Eng. C 48 (2015) 287-293.

[46] J. Njagi, S. Andreescu, Stable enzyme biosensors based on chemically synthesized Au-polypyrrole nanocomposites, Biosens. Bioelectron. 23 (2007) 168-175.

[47] K. Xue, S. Zhou, H. Shi, X. Feng, H. Xin, W. Song, A novel amperometric glucose biosensor based on ternary gold nanoparticles/polypyrrole/reduced graphene oxide nanocomposite, Sens. Actuators B 203 (2014) 412-416.

[48] J. Li, X. Lin, Glucose biosensor based on immobilization of glucose oxidase in poly(o-aminophenol) film on polypyrrole-Pt nanocomposite modified glassy carbon electrode, Biosens. Bioelectron. 22 (2007) 2898-2905.

[49] R.A. Kamin, G.S. Wilson, Rotating ring-disk enzyme electrode for biocatalysis kinetic studies and characterization of the immobilized enzyme layer, Anal. Chem. 52 (1980) 1198-1205.

[50] F. Arslan, S. Ustabaş, H. Arslan, An amperometric biosensor for glucose determination prepared from glucose oxidase immobilized in polyaniline-polyvinylsulfonate film, Sensor, 11 (2011) 8152.

[51] J.C. Vidal, E. Garcia, J.R. Castillo, Electropolymerization of pyrrole and immobilization of glucose oxidase in a flow system: influence of the operating conditions on analytical performance, Biosens. Bioelectron. 13 (1998) 371-382.

[52] R. Ahmad, M. Vaseem, N. Tripathy, Y.-B. Hahn, Wide Linear-Range Detecting Nonenzymatic Glucose Biosensor Based on CuO Nanoparticles Inkjet-Printed on Electrodes, Anal. Chem. 85 (2013) 10448-10454.

Figure captions

Fig. 1 Schematic of glucose biosensor fabrication strategy showing MWCNTs functionalization with carboxylic groups, electrochemical polymerization on GCE after adding fMWCNTs, pyrrole monomers and Nf, and CH-GOx immobilization, respectively.

Fig. 2 FESEM images of bio-nanohybrid composites used for electrode fabrication. (a) only PPy, (b) PPy-fMWCNTs, (c) PPy-Nf-fMWCNTs, (d) CH-GOx/PPy, (e) CH-GOx/PPy-fMWCNTs, and (f) CH-GOx/PPy-Nf-fMWCNTs. Inset d, e and f show the EDX analysis of CH-GOx immobilized on PPy, PPy-fMWCNTs and PPy-Nf-fMWCNTs, respectively.

Fig. 3 Low (a) and high (b) resolution Cs-Corrected-FETEM/STEM image of fMWCNTs with PPy and (c) mapping of PPy decorated fMWCNTs.

Fig. 4 FT-IR spectra of (a) fMWCNTs, (b) electropolymerized PPy, and (c) PPy-Nf-fMWCNTs nano-hybrid composite.

Fig. 5 Raman spectra of (a) fMWCNTs, (b) electropolymerized PPy, and (c) PPy-Nf-fMWCNTs nano-hybrid composite at λ=488nm.

Fig. 6 UV-Visible absorption spectra of (a) fMWCNTs bundles, (b) electropolymerized PPy, and (c) PPy-Nf-fMWCNTs nano-hybrid composite.

Fig. 7 Nyquist plots of the GCE modified electrodes with (a) CH-GOx/PPy, (b) PPy, (c) CH-GOx/PPy-fMWCNTs, (d) PPy-fMWCNTs, (e) CH-GOx/PPy-Nf-fMWCNTs, and (f) PPy-Nf-fMWCNTs in 0.1M PBS (pH 7.4). An upper and lower inset shows the equivalent circuit and an enlargement for the high-frequency plots, respectively.

Fig. 8 (a) CV responses of the CH-GOx/PPy-Nf-fMWCNTs/GCE biosensor electrode in 0.1 M

PBS containing redox mediator (5 mM $[Fe(CN)_6]^{3-/4-}$ with 0.1 M KCl) at different scan rates and (b) Variation of anodic and cathodic peak currents as a function of square root of the scan rates.

Fig. 9 CVs of (a, b) CH-GOx/PPy/GCE, (c, d) CH-GOx/PPy-fMWCNTs/GCE, and (e, f) CH-GOx/PPy-Nf-fMWCNTs/GCE biosensor electrodes measured in the absence (dash lines; a, c, and e) and presence of 2.0 mM glucose (solid lines; b, d, and f), respectively, in 0.1 M PBS (pH 7.4) at the scan rate of 50 mV/s.

Fig. 10 (a) Amperometric response of the CH-GOx/PPy-Nf-fMWCNTs/GCE electrode with successive addition of different concentrations of glucose at +0.25 V (*vs.* SCE) in 0.1 M PBS and (b) corresponding calibration curve. The inset of figure (a) and (b) show its current response towards 5 μM glucose and the Lineweaver-Burk plot, respectively.

Fig. 11 (a) Interference test of fabricated biosensor with successive addition of 1.0 mM glucose, 0.5 mM of each interfering species i.e. AA, DA, UA, and 1.0 mM glucose, respectively in 0.1 M PBS at +0.25 V (*vs.* SCE); (b) The histogram showing long-term stability measurement of CH-GOx/PPy-Nf-fMWCNTs/GCE electrode for 45 days.

Table 1. Comparison of analytical performance with previously reported PPy modified GCE-based glucose biosensors.

Working electrode	**Sensitivity** ($\mu Acm^{-2} mM^{-1}$)	K_M^{app} **(mM)**	**LOD (μM)**	**Linear range (mM)**	**Ref.**
GOx/PPy/GCE	-	0.045	-	.06-0.25	[44]
GOx-CH/PPy-Au NPs/GCE	0.58	1.83	68	1-20	[45]
GOx/Au-PPy/GCE	1.089	-	2.1	0.0025-5	[46]
GOx-CH/AuNPs/PPy/RGO/GCE	123.8	-	-	0.2-1.2	[47]
GOx/PPy NWs-Pt/GCE	9.9	23.9	0.45	0.0015-13	[48]
GOx/PPy NWs/GCE	3.5	6.9	0.95	0.0055-12	[48]
CH-GOx/PPy-Nf-fMWCNTs/GCE	2860.3	0.034	5	0.01-4.7	This work

Table 2. Determination of glucose in human serum samples.

Samples	Glucose concentration in serum sample (mM)	RSD (n=5) (%)	Added pure glucose (mM)	Recovery of added glucose (%)
1	0.49	3.2	1.0	97
2	0.98	2.6	1.0	96
3	2.45	1.9	1.0	98

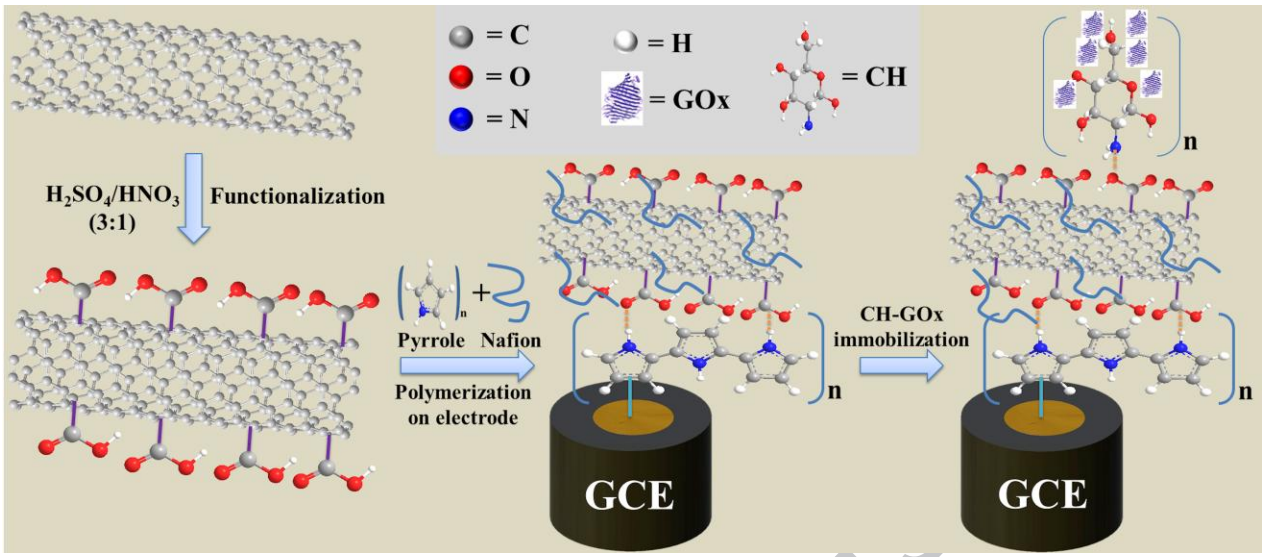

Fig. 1/11

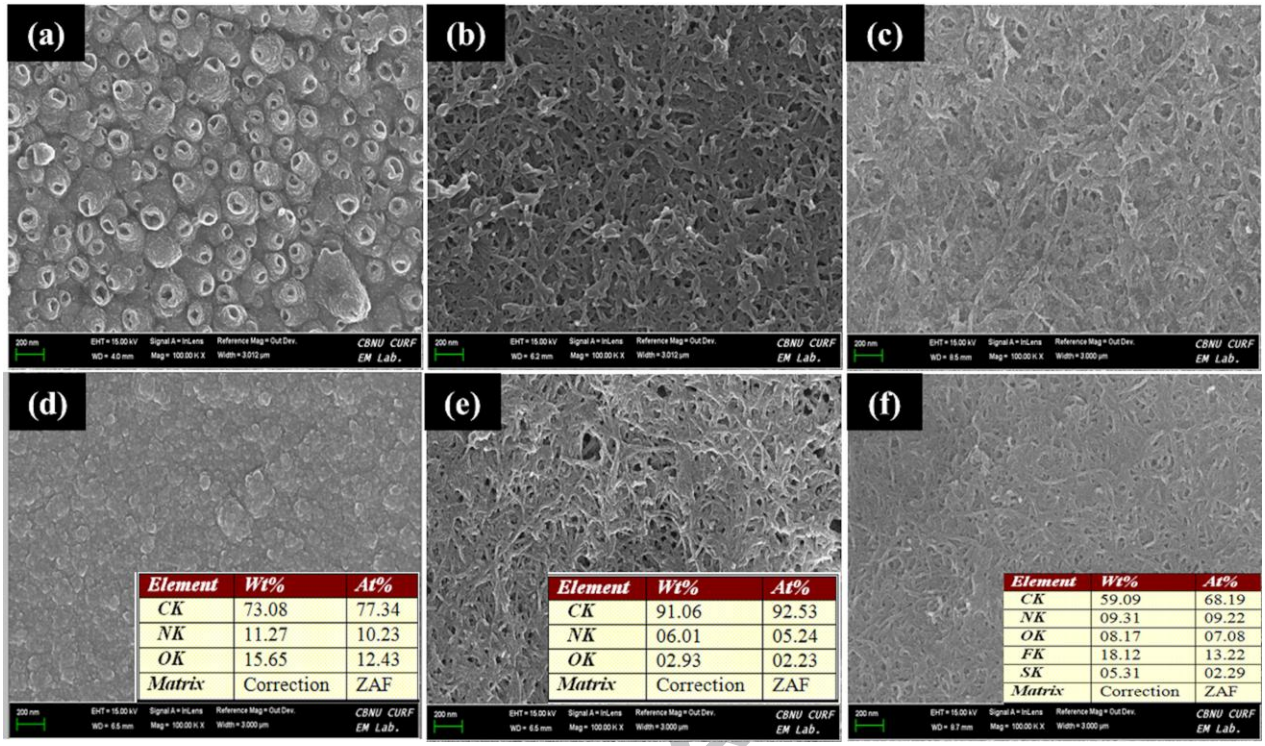

Element	Wt%	At%
CK	73.08	77.34
NK	11.27	10.23
OK	15.65	12.43
Matrix	Correction	ZAF

Element	Wt%	At%
CK	91.06	92.53
NK	06.01	05.24
OK	02.93	02.23
Matrix	Correction	ZAF

Element	Wt%	At%
CK	59.09	68.19
NK	09.31	09.22
OK	08.17	07.08
FK	18.12	13.22
SK	05.31	02.29
Matrix	Correction	ZAF

Fig. 2/11

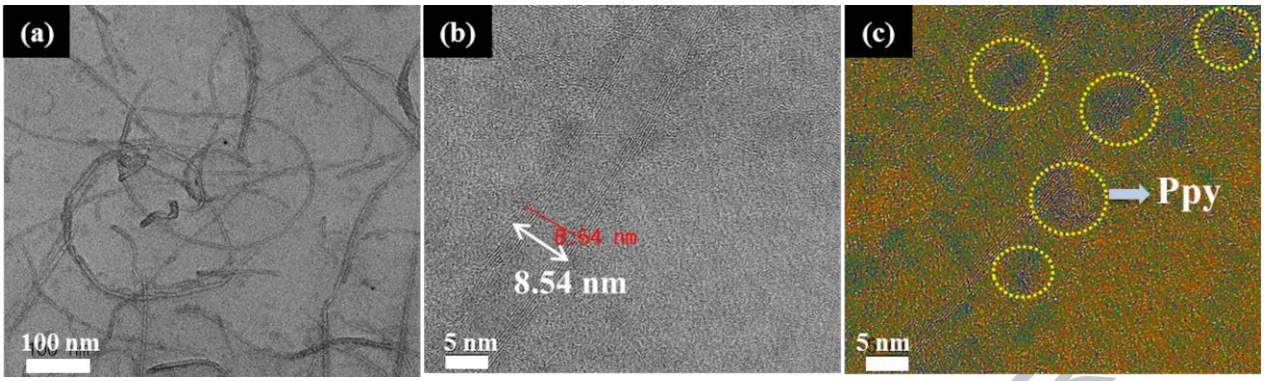

Fig. 3/11

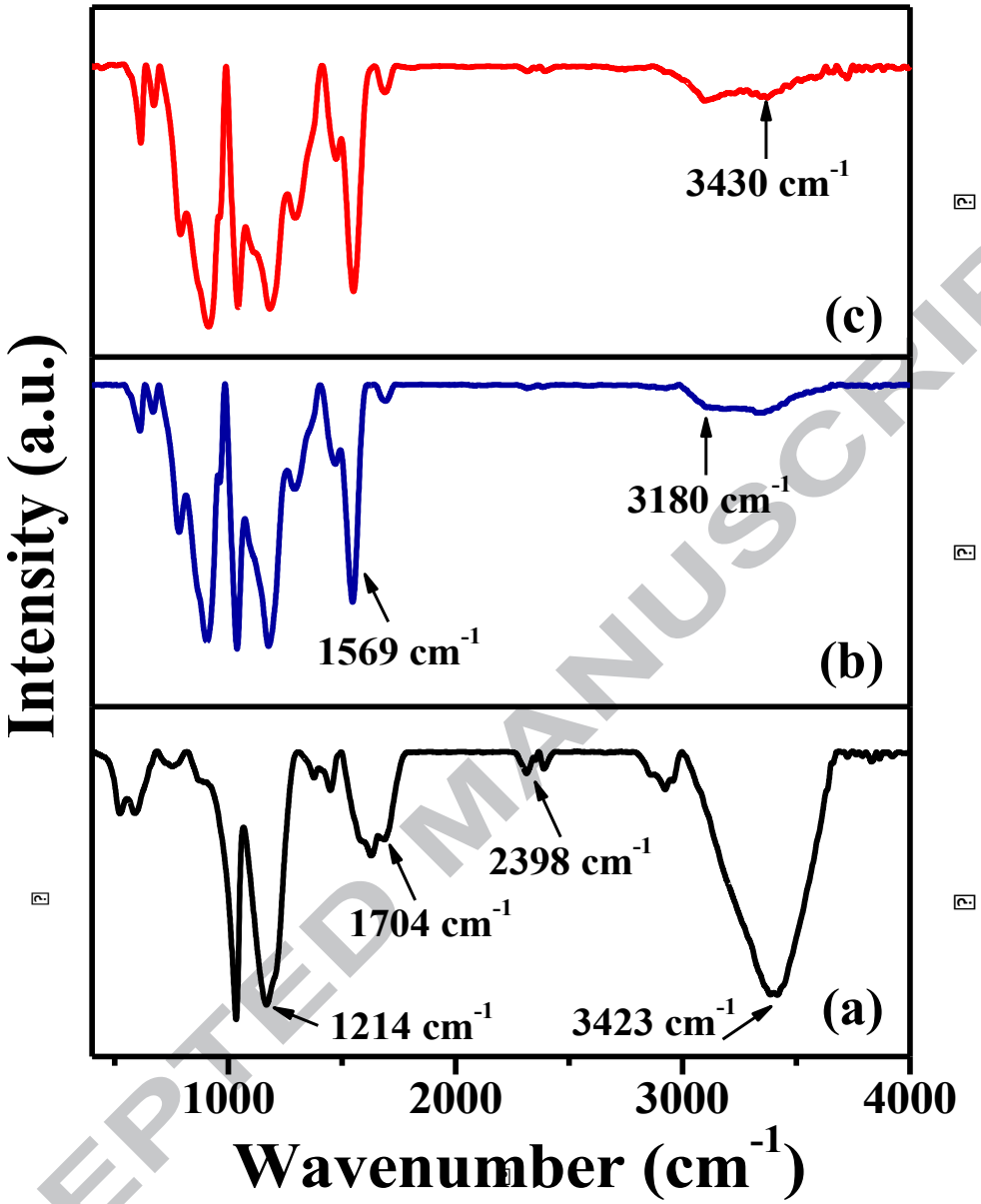

Fig. 4/11

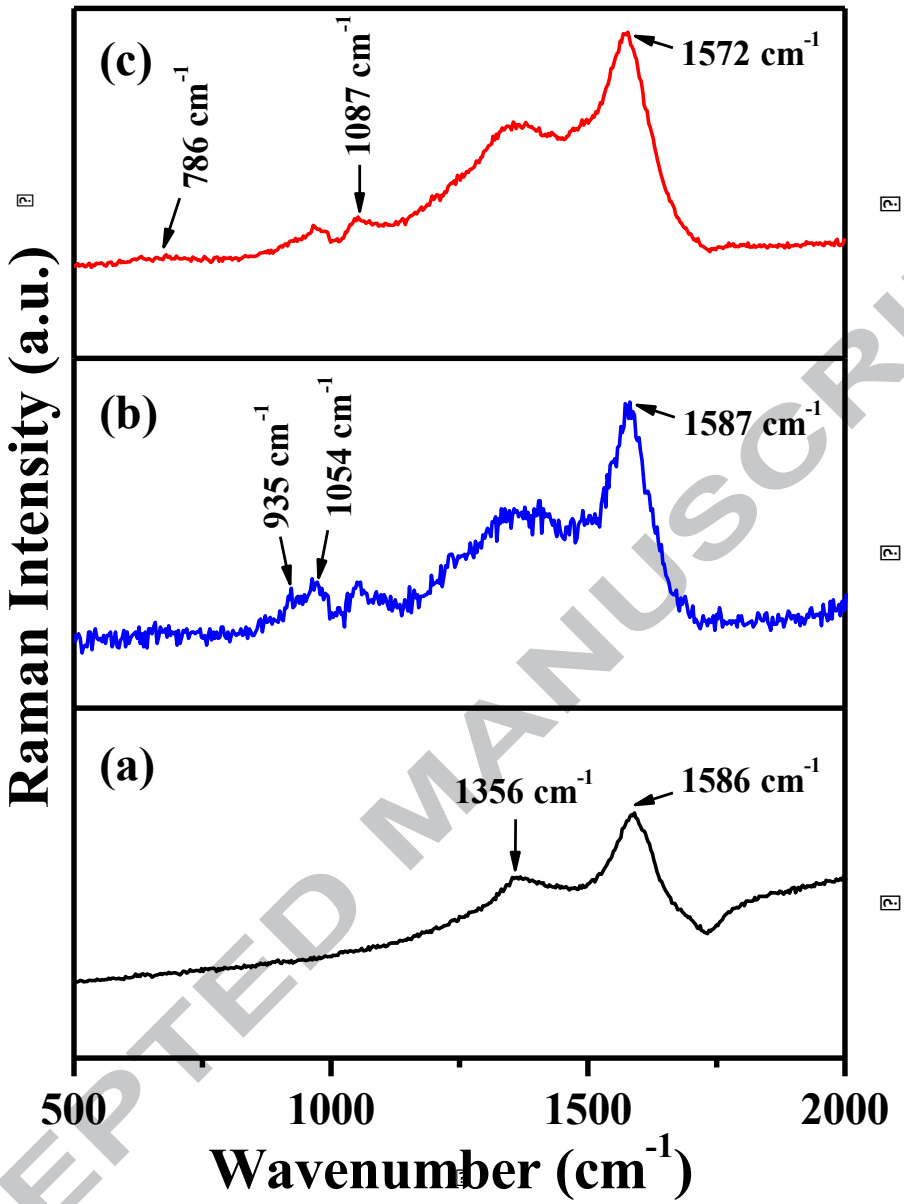

Fig. 5/11

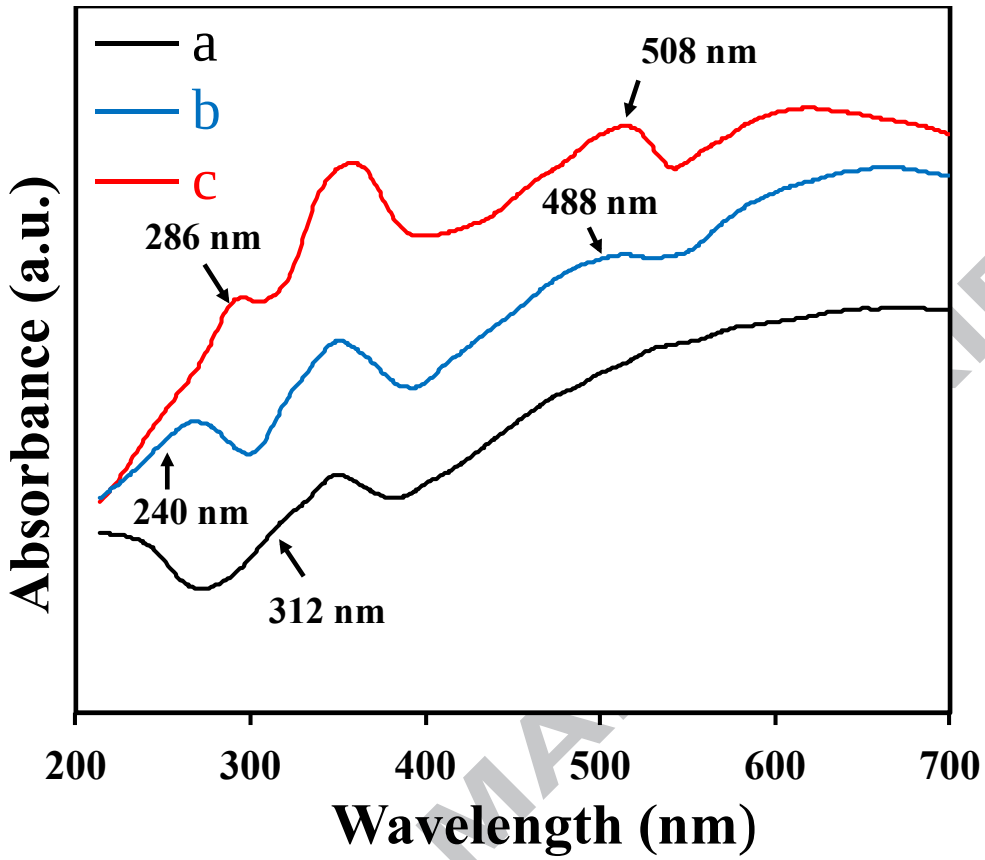

Fig. 6/11

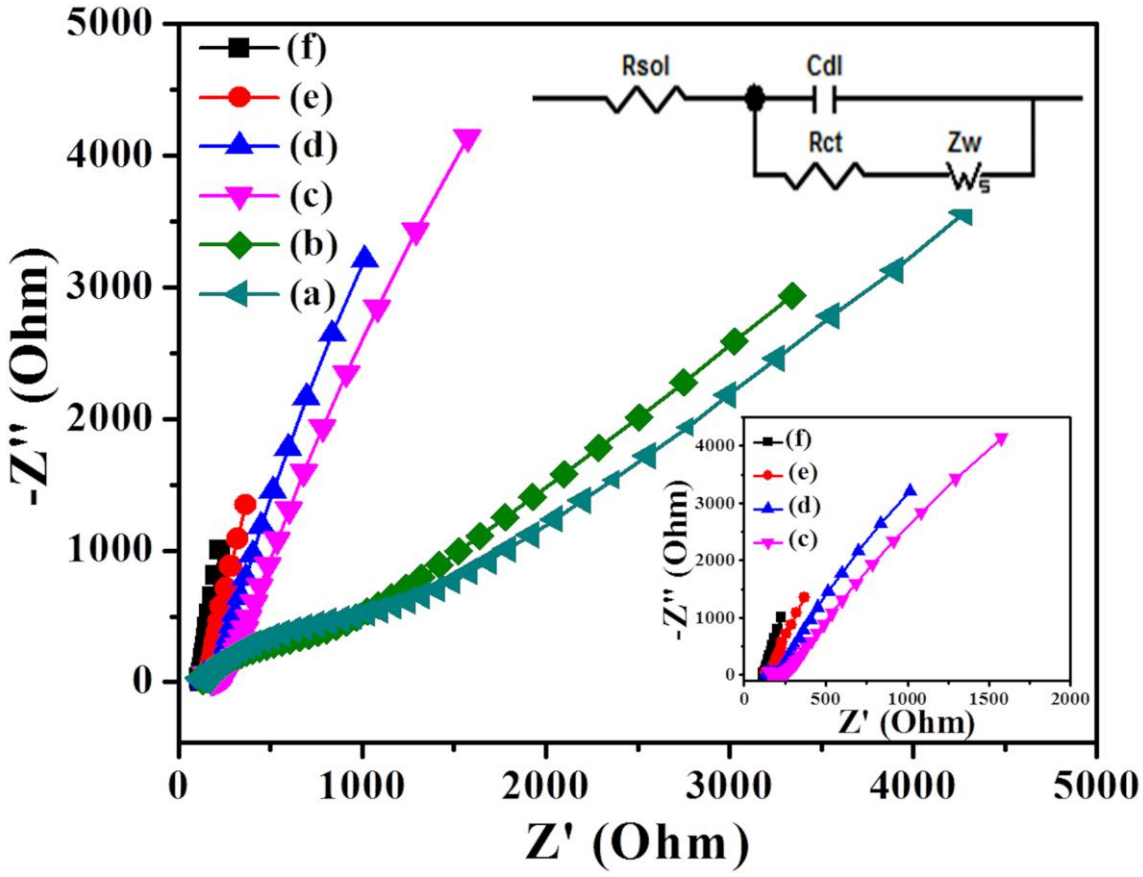

Fig. 7/11

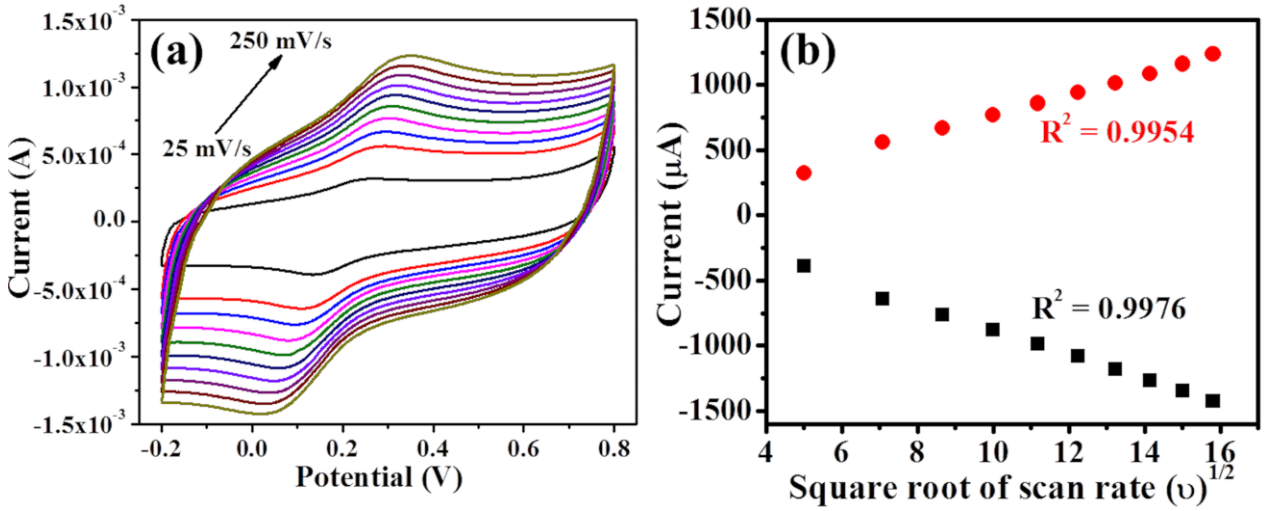

Fig. 8/11

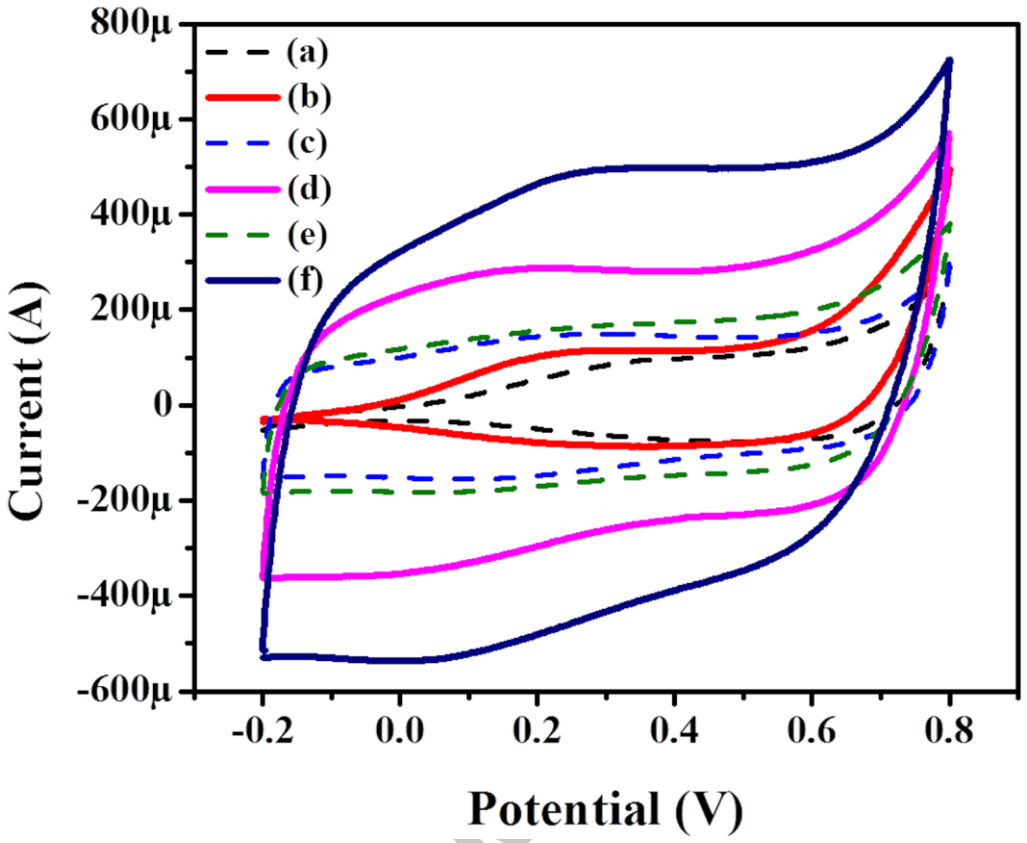

Fig. 9/11

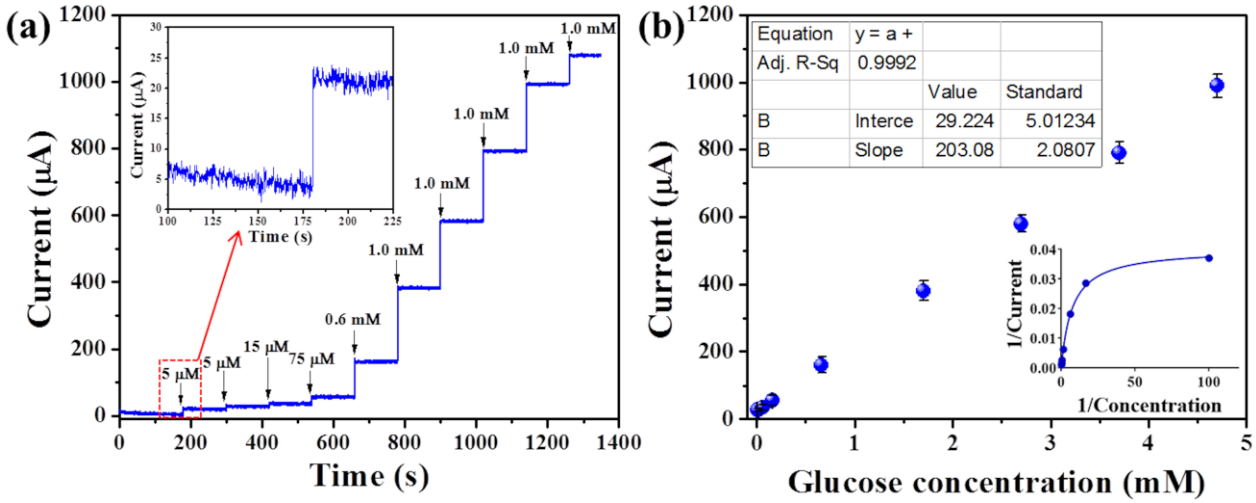

Fig. 10/11

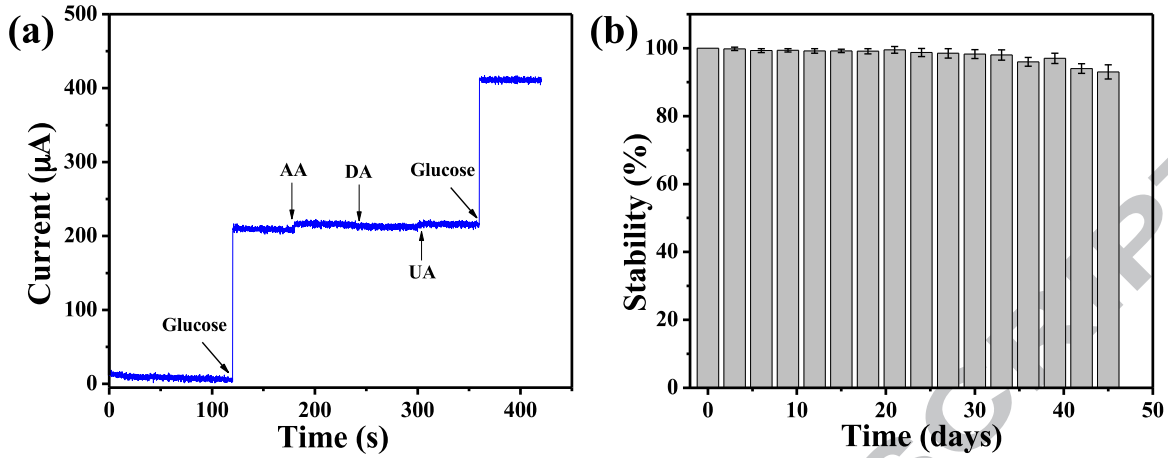

Fig. 11/11

Graphic Abstract